SANDSAND2017-13807J

Shock Interactions with Heterogeneous Energetic Materials

Cole D. Yarrington* and Ryan R. Wixom

Sandia National Laboratories, Albuquerque, New Mexico 87185, USA

(Dated: December 20, 2017)

Abstract

The complex physical phenomenon of shock wave interaction with material heterogeneities has significant importance and nevertheless remains little understood. In many materials, the observed macroscale response to shock loading is governed by characteristics of the microstructure. Yet the majority of computational studies aimed at predicting phenomena affected by these processes, such as initiation and propagation of detonation waves in explosives, or shock propagation in geological materials, employ continuum material and reactive burn model treatment. In an effort to highlight the grain-scale processes that underlie the observable effects in an energetic system, a grain-scale model for hexanitrostilbene (HNS) has been developed. Measured microstructures were used to produce synthetic computational representations of the pore structure, and a density functional theory molecular dynamics (DFT-MD) derived equation of state (EOS) was used for the fully dense HNS matrix. The explicit inclusion of microstructure along with a fully-dense EOS resulted in close agreement with historical shock compression experiments. More recent experiments on dynamic reaction threshold were also reproduced by inclusion of a global kinetics model. The complete model was shown to reproduce accurately the expected response of this heterogeneous material to shock loading. Mesoscale simulations were shown to provide clear insight into the nature of threshold behavior, and are a way to understand complex physical phenomena.

I. INTRODUCTION

Shock wave theory has a rich and interesting history dating back to the late 1800s, when scientists were developing the basic mathematical framework and debating (for several decades) the possible existence of what we now refer to as a shock wave. It was only later realized that the "Rankine-Hugoniot" equations were a special and limiting case of the Navier-Stokes equations.[1] Unfortunately, like many specific applications of fluid dynamics, the assumptions making the mathematics tenable are quite constraining. So, while the propagation of a 1-D shock through a uniform gas is reasonably well described, that same level of accuracy does not necessarily hold for a shock moving through real materials where heterogeneities play a role. The magnitude of heterogeneous effects depends on the relative values of factors like shock magnitude, material viscosity or strength, and length scale of the heterogeneities.

A comprehensive understanding of how shock waves propagate through real materials is perhaps more technologically valuable than many believe. Consider that one of the most profitable inventions of all time, dynamite, was based on Alfred Nobel's understanding that bubbles in nitroglycerine were responsible for its sensitivity to mechanical insult. The oil industry uses shock wave theory to locate and extract valuable product. Considering the vast scale of these operations, it is not surprising that targeted research efforts that result in even modest efficiency gains could have large economic impacts. For example, during oil well completion, there are inefficiencies related to the shock/sandstone/limestone interaction with significant implications for recovery of hydrocarbons from the well. The interaction of shock waves with these heterogeneous materials could be better understood through simulations at the microscale and ideally those simulations would be used to formulate and parameterize continuum penetration models and damage models.[2]

In the field of explosives, so called "hot spot theory" has been used to describe the initiation and growth of chemically sustained shock waves, or detonation waves, since 1952.[3] While this theory provides a useful framework for describing initiation, the specifics of detailed microstructure interactions with shocks are not treated. Experimental efforts focused on discovering correlations between specific microstructural measures and observable trends were successful in finding links between powder characteristics (specific surface area, grain size), and dynamic properties (critical diameter, gap/shock sensitivity).[4–7] Readily avail-

able highly resolved scanning electron microscope (SEM) micrographs of explosives now enable the study of explosive properties with respect to underlying as-pressed microstructural characteristics. Understanding the physics, as opposed to the observational or empirical understanding, of how microstructure affects explosive material performance is likely to be a significant research topic in the near term for energetic materials practitioners. While the use of stochastic materials have been necessary due to the available manufacturing and processing methods, they are much more complex than proposed "prescribed microstructure" materials made possible through advanced manufacturing techniques. By coupling enhanced understanding of the shock/heterogeneous material interaction with these advanced manufacturing techniques, one could imagine a number of achievable and desirable technologies such as precision arrays of void space used to attenuate shock strength, tailored explosive sensitivity, or shock energy focusing with unprecedented control.

The numerical simulation of shock interaction with heterogeneous features using a continuum framework began as early as 1965 with work by Mader on single pores and density discontinuities in nitromethane. This work provided the first numerical evidence of possible mechanisms of hot spot formation. Mader predicted the formation of a hot spot and both detonation and failure depending on the piston velocity.[8] Mader also investigated the source of detonation failure, and determined that side rarefractions cooled the explosive sufficiently to induce failure in the reaction zone.[9] Multiple void interactions were investigated by Williamson[10] where the shock interaction with uniformly sized cylindrical grains and the associated pore space were simulated, and evidence for particle melting and bonding at interfaces was found at high impact stresses. The addition of nonuniform particle size distributions was investigated by Benson and Nellis, where a size distribution of copper spheres is compacted using a pseudo-gravity method, and subjected to shock loading.[11] A series of papers by Baer et al. began to look at the shock loading of three-dimensional realistic explosive microstructures.[12–16] Several important insights were brought to light in these studies, including: 1) shock focusing at particle interfaces results in plastic work and the formation of hot spots, and this is enhanced by multiple crystal interactions,[13] 2) several temperature regions can be identified in the temperature states associated with elastic response, bulk response, grain interactions, and hot spots,[14,15] 3) the interaction of shock waves with heterogeneous material structures is inherently non-equilibrium and reactions initiated at larger crystals are less affected by edge rarefractions, and 4) hot spots scale directly with feature

size. Reaugh predicted critical hot spot diameters from bimodal mesoscale assemblies of HMX crystals subjected to shock pressures of 2.5 GPa and 10 GPa as 250 nm and 170 nm, respectively.[17] Grain representations obtained through Voronoi tesselation techniques have been employed to match HMX grain size distributions through shock impact simulations and subsequent interrogation of the temperature fields. Multiple instantiations of these microstructures were used to obtain statistics on the temperature distribution, and ultimately to predict threshold sensitivity based on published critical hotspot criterion.[18–21]

One area that has not been widely utilized, due to the limitations of computational resources, is that of large-domain calculations with length scales on the order of observed phenomena, such as the run-to-detonation distance. Baer highlighted the importance of including the coupled effects of collections of pores as opposed to a single pore, and this will be done on a much larger scale. It will be shown that, with appropriate inclusion of microstructure and fully dense material properties, these models are capable of modeling the run-up to or failure of detonation as a function of the impact conditions.

II. HNS REVIEW

While the topic of shock interaction in heterogeneous materials is sufficiently general to justify the study of any porous material, a choice was made to focus on a single explosive with characteristics that make it a suitable test material. Hexanitrostilbene (HNS) is widely used in explosive applications due to its relative stability at moderate temperatures and high impact sensitivity, and it is often pressed neat without the use of binders or additives. These properties make it an ideal material for study of mesoscale phenomena in impact initiated applications. It was recognized early on that due to the many grades of HNS there would be differences in sensitivity and performance due to microstructural properties. Schwarz[22,23] showed that HNS with smaller particle sizes resulted in shorter run-to-detonation distances, and lower critical energies under sustained impulse conditions. Setchell[24] showed a reverse of this trend under different experimental conditions. Recently, any dependence on microstructure has been called into question by Harris et al.,[25] who also highlighted the importance of the choice of solvent during the washing step of high surface area HNS. The conclusions reached in the referenced studies often discount the effect that processing has on the final microstructure of the test specimens by discussing results only in terms of the initial powder

characteristics and the pressed compact bulk density. This omission is critical as the pressed microstructure of the test specimens ultimately affects hot spot formation and impact sensitivity. Clearly, there still exists a fundamental gap in understanding of the observable effects of powder and pellet microstructure on performance, and the mechanisms that could explain these effects.

Brundage et al.[26] conducted mesoscale modeling simulations of HNS by importing the measured three-dimensional microstructure of pressed pellets of HNS directly into CTH,[27] Sandia's Eulerian finite-volume shock physics code. In other studies, he used continuum multiphase mixture theory to reduce the computational cost of the three-dimensional mesoscale treatment, and showed that the predicted shock sensitivity of HNS is sensitive to uncertainty in the unreacted equation of state (EOS).[28–30] The lack of an unreacted EOS for crystalline HNS has been a significant obstacle to predicting the dynamic response of HNS. Although others have used EOSs obtained through various experiments using porous HNS, this technique yields only estimates that are subject to numerous assumptions.[29] EOS data obtained through experiments on actual HNS single crystals has remained out of reach due to the difficulty in synthesizing large enough samples.

More recently, Mattsson et al. developed an ab-initio method for determining the EOS of molecules in crystal lattices which was applied to PETN.[31] Using this technique, the difficulties in obtaining the EOS for crystalline HNS by experiment can be bypassed and the result obtained on theoretical grounds, subject to experimental validation. As indicated by Brundage, the unreacted EOS plays a large role in the sensitivity of the dynamic shock properties of HNS.[30] Employing an EOS based on first principles allows for interpretation of results from mesoscale simulations in more than a descriptive sense, and moves the method one step closer to predictive.

III. HNS MICROSTRUCTURE

Several different grades of hexanitrostilbene (HNS) powders are commercially available, such as HNS-I and HNS-IV. Examples of these particular grades are shown in the SEM micrographs in Fig. 1. Qualitatively, one can see that these grades of HNS are very different, with HNS-IV having a more needle-like appearance, and HNS-I appearing more platelet like. Furthermore, different lots can often exhibit large variation as well, as seen in the two

FIG. 1: SEM images of HNS with different particle morphology and size. (top/middle) Two different lots of HNS-IV showing lot to lot variation which leads to significant shifts in threshold. (bottom) HNS-I. Common scale bar shown.

images of HNS-IV from different lots. Previously, researchers have focused on demonstrating the dependence of sensitivity and shock-to-detonation transition (SDT) mechanisms on loose powder properties such as the initial particle size and distribution, and experimental variables such as the shock loading magnitude and flyer thickness[22–24,32–35] One unknown in studies of this kind is the effect of the manufacturing processes that led to the high density,

as-tested samples. While methods such as the discrete element method make progress on modeling the manufacturing of samples,[36,37] extensive characterization of the pressed samples allows for parallel efforts to proceed on the dynamic response of materials, correlating performance to the more relevant properties of pellets as opposed to powders. In the study presented here, loose HNS powder with measured specific surface area (SSA) of 6.0 m^2/g was pressed to a density of 1.6 g/cm^3, or 92% of theoretical maximum density (TMD), and the pressed samples were then used for characterization and dynamic testing. Two-dimensional characterization of the pellet microstructures was carried out on sample images obtained by ion-mill cross-sectioning and subsequent SEM imaging.[32] The methodology followed for incorporating this characterization into a dynamic model will be discussed in the following section.

IV. MODELING APPROACH

A. Simulated Microstructure

While it is possible to perform dynamic impact simulations on computational microstructures directly imported from post-processed SEM images, much can be gained through use of a simulated microstructure that can be modified with little effort. A simulated microstructure yields itself to tractable and systematic variations on the microstructure that can be used to study more general trends applicable to a wider range of materials. By employing a 2D assumption, significant savings in computational cost are gained that are necessary to complete simulations on initiation length scales. These gains come at the expense of some accuracy, which is manifest largely in the temperature field. Ultimately these discrepancies are homogenized through use of the global reaction kinetics model, and the conclusions can be applied generally. The methodology used in preparing two-dimensional (2D) reconstructed microstructures for use in impact simulations was to match three statistical parameters as closely as possible while using non-contacting circles as a 2D pore model (the circles are effectively cylinders with infinite extent in the 2D simulations). Bourne and Milne[38] investigated pore collapse in ammonium nitrate of different void shapes, however the effect of shape on sensitivity was beyond the scope of their study. It is assumed here that by using a large enough domain, pore shape effects will be minimized and the cylindrical model will

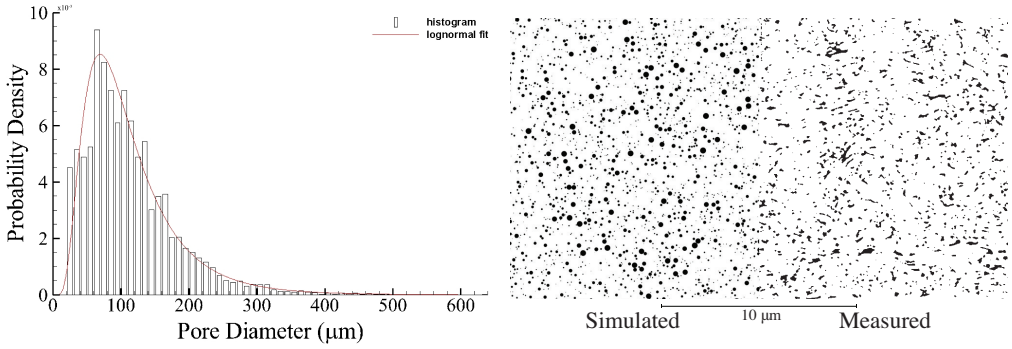

FIG. 2: PSD and threshold images. (left) Probability density of pore diameter and log-normal distribution fit. (right) Measured and reconstructed HNS planar microstructure. Black represents void space, and white represents fully dense HNS.

be sufficient for observations regarding sensitivity and changes in pore distribution.

Obtaining an effective circular pore size distribution (PSD) from 2D planar images was done using common image processing techniques. The high resolution grayscale SEM images were threshold segmented resulting in images where the pores and HNS matrix had binary pixel values. The area of each pore and the corresponding effective circular diameter were each calculated and binned. Several distributions were applied to the histogram, and the log-normal resulted in the best fit, and was used in subsequent microstructure reconstruction. The 2D PSD log-normal fit was then used to populate a domain with circular, non-contacting pores with periodic side boundaries enforced, until the measured porosity was reached. Figure 2 shows a PSD histogram and log-normal fit, as well as threshold images of cross-sectioned samples and a simulated cross-section.

Images were reconstructed based on this domain, and the distribution was then modified to minimize the error between simulated and measured values of two additional parameters: (1) two point probability function, S_2; and (2) lineal path function (see Fig. 2 and Fig. 3). These parameters are defined in Torquato[39] as

$$S_2^{(i)}(r) = P\left[I^i(\vec{x}_1 = 1, \vec{x}_2 = 1)\right], \text{ and} \tag{1}$$

$$L^i(r) = \textit{Probability that a line segment of length } r \textit{ lies wholly in phase } i \textit{ when randomly thrown into the sample.} \tag{2}$$

In the above equations r is the distance between $\vec{x}_1$ and $\vec{x}_2$ in S_2, or the length of the line

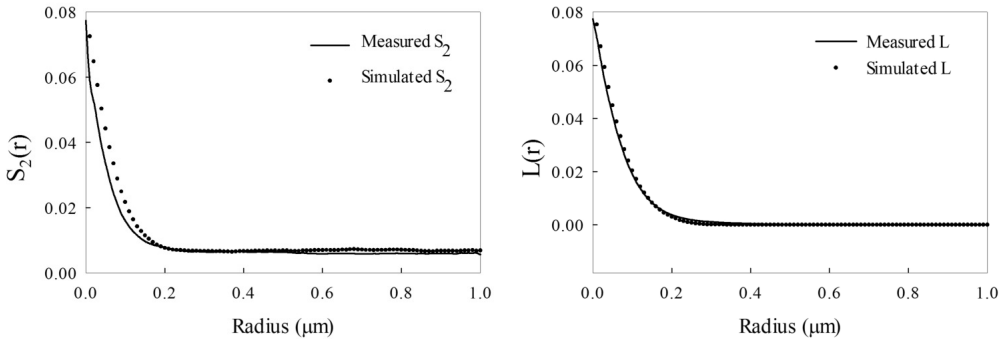

FIG. 3: Microstructural statistics for measured and simulated HNS. (left) Two point probability function. (right) Lineal path function.

in L, $\vec{x}_1$ and $\vec{x}_2$ are random points in the domain, I^i is a binary phase value where 1 is a phase positive, and 0 is a phase negative, and i is the phase index. S_2 can also be described as the probability that any two randomly chosen points are in the same phase. Finally, with the location and size of each pore defined, material insertion and deletion algorithms were used to add material and create porosity in the computational domain by removing the circular pores from an initially solid block of material.

B. Hydrocode and DFT Modeling

CTH,[27] a multi-material, large deformation, strong shock wave, solid mechanics code developed at Sandia National Laboratories, was used to model a high velocity impact scenario of a thin flyer onto the mesoscale reconstruction of HNS described previously. Since the local porosity of HNS was modeled explicitly, the HNS matrix was assumed to be fully dense, and required the development of a new EOS. A first principles approach using density functional theory molecular dynamics (DFT-MD) was adopted to predict the unreacted principal Hugoniot of fully dense HNS. These techniques have been shown to provide extremely accurate predictions of the unreacted Hugoniot for a wide variety of materials.[40–42] The calculations, utilizing the AM05 functional,[43] were performed with the Vienna ab-initio simulation package (VASP 5.2),[44–46] using strictly converged settings.[47] The plane-wave cutoff was set to 800 eV and k-point sampling with mean-value point (1/4, 1/4, 1/4) was used. The ionic time-step was set to 0.4 femtoseconds. The reference state was taken to be the experimental structure and volume for crystalline HNS.[48]

Points along the Hugoniot were found by setting the volume (V < V0) and equilibrating by running an NVT simulation (Nose-Hoover thermostat) for up to 10 ps. The temperature of that cell was then instantly increased in order to run several additional NVT trajectories at elevated temperatures. The pressure and energy from equilibrated portions of these runs were then used to write equations for $U(T)$ and $P(T)$. These equations, and the conservation of energy Rankine-Hugoniot relation,

$$U\left(T\right) - U_0 = \frac{1}{2}\left[P\left(T\right) + P_0\right]\left[V_0 - V\right], \tag{3}$$

were used to solve for the temperature on the Hugoniot. That temperature was then used to determine the pressure and energy on the Hugoniot for that set volume. Repeating this with increasing densities allows one to map out the unreacted Hugoniot to very high pressures, much higher than is achievable with flyer-impact experiments.

This method provides everything that is needed to define an EOS surface. For this initial work, the P-V Hugoniot was transformed to U_s-u_p space and fit to the second order polynomial shown in Eq. 4. Finally, this quadratic U_s-u_p relationship was used along with physical properties of HNS to parameterize a Mie-Gruneisen EOS[49] for the reactants. An existing tabular EOS[50] was used for the HNS products.

$$\begin{gathered} U_s = Au_p^2 + Bu_p + C \\ A = -0.113\ (s/km) \\ B = 1.853\ (dimensionless) \\ C = 2.761\ (km/s) \end{gathered} \tag{4}$$

In modeling stochastic processes like hot spot formation and the coalescence of wave disturbances due to heterogeneities, adequate statistical sampling can be achieved by either a large number of experiments with different samples, or a single sample of large enough size called a representative volume element (RVE). The RVE has the advantages of containing enough microstructure to be representative, and yet being smaller than the characteristic macroscopic length scale, resulting in reasonable computational cost. The minimum RVE size was estimated by producing a number of random reconstructed microstructures and running flyer impact simulations. The material response was analyzed in terms of mean and

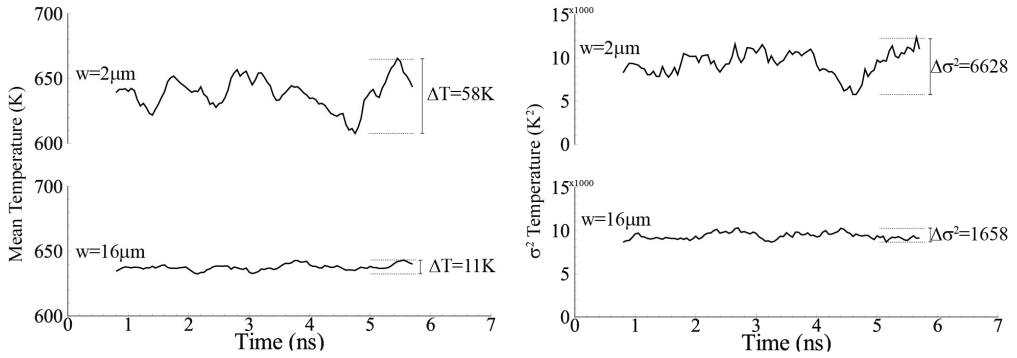

FIG. 4: Temperature (left) mean and (right) variance for two domain sizes.

variance, and a minimum domain size was determined where the increasing domain size no longer affected the response.

Plotted in Fig. 4 is the time history of the temperature mean and variance of a region trailing the shock front with dimensions of 2 μm by full-width. When the computational domain width is less than 16 μm, the variation in mean and variance is greater than 1%, so the minimum RVE size is determined to be 16 μm. For reactive flow simulations, the consequence of using a domain smaller than the RVE would be greater uncertainty of results, which in turn can result in predicting erroneous threshold values. This would more acutely affect prediction of unstable phenomena, such as SDT threshold. For example, if a temperature-dependent Arrhenius based reactive burn model were used, even a temperature difference of a few K can make a significant difference in threshold predictions. A grid refinement study led to the determination that a cell size of 8 nm was sufficient to accurately represent the material response for this distribution.

V. RESULTS

A. Predicted Inert Response

A mesoscale model must accurately predict the inert response to ensure confidence in its use in a fully reactive model. Although there are EOSs available for unreacted HNS, the experiments performed to parameterize them are almost exclusively done with pressed porous samples and provide the continuum representation of the random heterogeneous material. The approach outlined in this paper does not rely on data fitting methods or

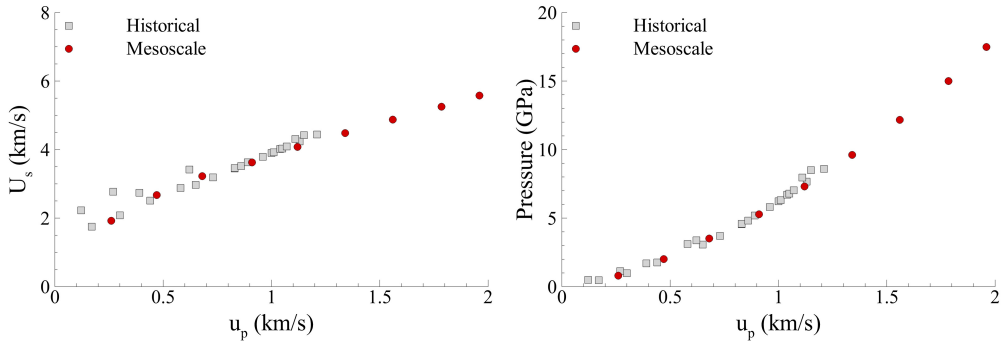

FIG. 5: Historical HNS Hugoniot data plotted with the mesoscale simulation results using the inert EOS.

experiments to obtain parameters, but rather the parameters result from the first principles analysis of DFT-MD and experiments are used to validate the model.[32] This model uses periodic boundary conditions, and so assumes a 1D flyer, consistent with the experimental flyer aspect ratio of ∼58:1. Model predictions of the Hugoniot were made by extracting the material shock dynamics from flyer impact simulations and comparing them to historical data. This was done by averaging the predicted state properties at 100 Lagrangian tracer points placed at the flyer/HNS interface. Figure 5 shows the predicted unreacted Hugoniot along with the historical data points.

Predictions of the distribution of temperatures due to heterogeneities were also made, however no experimental data currently exists for local hot spot temperatures of pressed HNS for comparison. It is likely that predicting accurate temperatures due to pore collapse is the limiting factor for this model in terms of being predictive, and progress in this area will be incorporated in future efforts.[51,52]

B. Reactive Burn Model

Reactive burn models (RBM) employed in continuum simulations, such as History Variable Reactive Burn (HVRB)[49] and Ignition and Growth (IG)[53] are phenomenological models fit to experimental data. These models often match specific aspects of heterogeneous explosive behavior very well once they are tuned to experimental data, and many of these models are predominantly dependent on a single state property which gives rise to their various designations: pressure, temperature, entropy dependent models, etc. However, when explicitly

modeling the porosity of a heterogeneous material, the application of a continuum RBM is not the most natural approach. The parameters of these continuum models are based on the very physical features that the mesoscale models attempt to predict, such as the production and subsequent growth and coalescence of hot spots, or the run distance to detonation. For these reasons, the Arrhenius reactive burn (ARB) model was chosen, which models the rate of chemical conversion as a function of the local temperature of the solid as shown in Eq. 5.

$$\begin{aligned} \dot{\lambda} = \frac{\mathrm{d}\lambda}{\mathrm{d}t} &= (1-\lambda)\, F \exp\left(-\Theta/T\right) \\ \Theta &= \Theta_0 \left(1 + A_P P\right) \end{aligned} \tag{5}$$

In Eq. 5, λ is the extent of reaction, F is the pre-exponential factor, T is temperature, and Θ is activation temperature. The model also includes a dependence on pressure through the definition of Θ, and the extra parameters Θ_0 and A_P are often determined through fitting experimental data. The temperature dependent Arrhenius form is used to model the reaction kinetics of the neat HNS in a single global step. Kipp and Setchell[54] developed a two term ARB model that matched experimental run distance data for sustained shock initiation of HNS. Using Kipp's model as a basis, single term Arrhenius parameters were determined by matching to experimental thin pulse SDT threshold data. In these results, it should be noted that the only parameter used for calibrating the burn model was F from Eq. 5. As research progresses on identifying the critical reaction mechanisms and rates following shock waves, including such discoveries in mesoscale models will result in increased fidelity and the ability to predict response based on fundamental input data, and experimental data on the bulk can be used for validation. The RVE was extended in length to include enough distance to simulate thin pulse SDT threshold experiments with an 11 μm thick flyer. Overlaid color maps of pressure, temperature, and extent of reaction at early time show the effects of microstructure on the fine scale structure of the state variables (see Fig. 6). In particular, the complex interaction of the initial shock wave with subsequent waves generated upon pore collapse is seen in the pressure maps. The result of these interactions is also seen in the temperature and extent of reaction, where energy localization led to concentrated regions of elevated temperature and reaction.

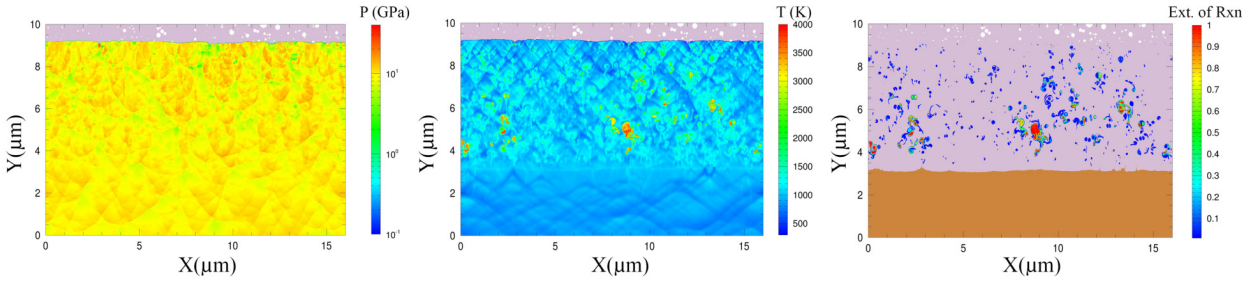

FIG. 6: Contours of pressure, temperature, and extent of reaction at 2.1 ns following impact of a flyer with velocity of 3.15 m/s.

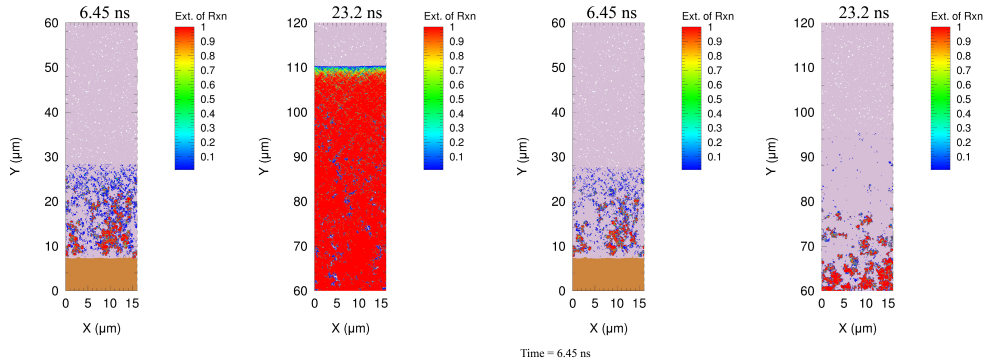

FIG. 7: Simulation images at early and late time and two different flyer velocities, (left) 3.15 km/s and (right) 3.05 km/s

VI. RESPONSE OF REACTIVE HNS

Simulation images from flyer impact at velocities of 3.15 and 3.05 km/s clearly show the initial reactions occurring behind the shock front (Fig. 7). In the 3.15 km/s case, these reactions continue even after the release wave overtakes the shock front, and the shock transitions to a steady detonation. In the 3.05 km/s case, the initial chemistry quenches due to the release wave, and the slightly reduced shock pressure resulting in lower hot spot temperatures on average. Because these flyer velocities were chosen near the experimentally observed threshold velocity, this behavior is expected, however simulations of this kind have not been reported previously due to the computational cost involved. The ability to capture a shock to detonation transition, and a failed initiation, will be a critical feature of energetic material mesoscale models going forward, as the technique is increasingly being called upon to inform microstructure aware continuum reactive burn models.

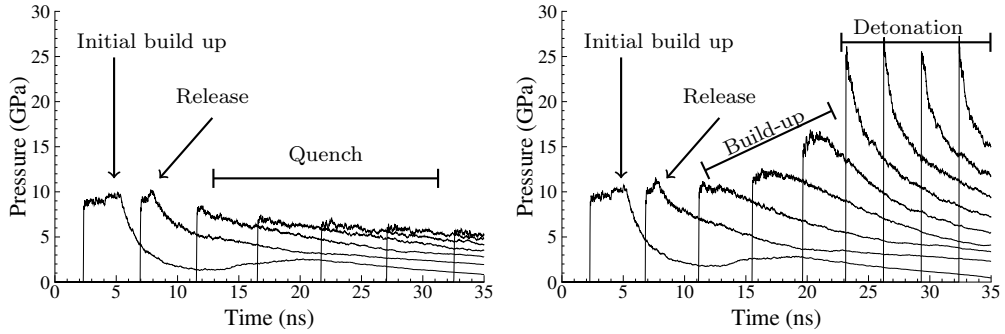

FIG. 8: Average pressure history of planes spaced 20 μm apart in the direction of shock travel. (left) Flyer velocity of 3.05 km/s, impact below threshold. (right) Flyer velocity of 3.15 km/s, successful SDT.

In Fig. 8 the time history of average pressure locations spaced 20 μm apart in the direction of the shock is shown for flyer impact velocities of 3.05 and 3.15 km/s. For the flyer velocity of 3.05 km/s, the pressure increases slightly at early times, but the rarefraction wave from the rear flyer surface prevents further build up to detonation. The decreasing pressure at later times is due to the regular dissipation of shock strength as it passes through the material. At a flyer impact speed of 3.15 km/s, hot spots form immediately after passage of the shock wave initially, and continue to form further into the sample. The release wave coming from the back of the flyer reaches the interface at around 10 ns and causes a momentary stall of pressure build up. At this flyer velocity, enough chemical energy has been released at this point to overcome the effects of the release wave, and at around 23 ns, a full transition to detonation has been reached with a run distance of 110 μm. The pressure traces also show that when SDT is achieved, the nature of the transition is characteristic of heterogeneous materials, with the pressure slowly increasing directly behind the shock front and eventually reaching a steady state. Typical homogeneous material behavior, resulting from thermal explosion and subsequent superdetonation waves was not seen in the simulations due to the shock magnitudes required to achieve initiation at such small flyer thicknesses. Setchell[55] observed that HNS behaved as a homogeneous explosive at lower pressure sustained pulse conditions, and comparing these results with the historical body of knowledge on HNS initiation, we conclude that the experimental conditions play a large role in the SDT behavior of HNS-IV, which can vary from homogeneous with sustained impulse, to heterogeneous for high shock strength, short pulse conditions (thin flyers).

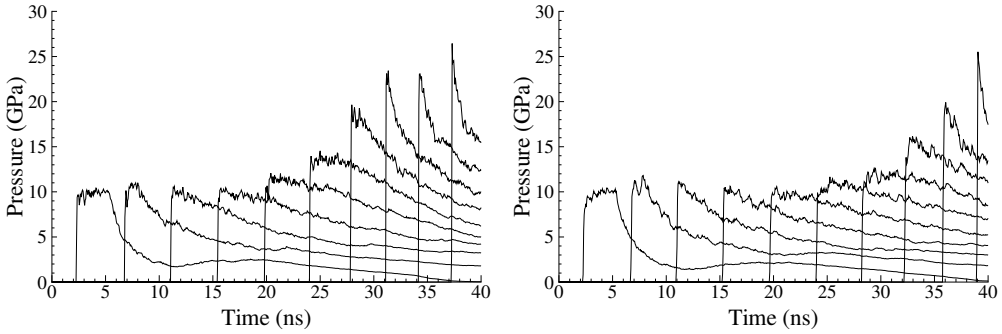

FIG. 9: Average pressure history for PSDs scaled up by factors of (left) 2 and (right) 4 showing increased run distance to detonation. The flyer velocity for this simulation was 3.15 km/s.

Although it is currently not known how the pore size distribution of pellets scales with HNS grade, simple estimates can be made to assess the impact of variable microstructure to performance. An estimate was performed for HNS by using the measured statistics of the PSD of HNS-IV, and assuming a linearly scaled self-similar distribution. This assumption results in a log-normal distribution that is essentially translated along the diameter axis by a factor, yet retaining shape relative to the mean. Pressure histories from flyer impacts on materials with simulated pore size distributions scaled up by factors of 2 and 4 revealed little difference at lower flyer velocities, with all cases failing to reach sustained detonation. At 3.15 km/s however, the larger pore size distributions resulted in sustained detonation but longer run distances (see Fig. 9), which is consistent with experimental results.[4]

VII. SUMMARY AND CONCLUSIONS

A mesoscale model for pressed HNS has been developed using microstructural data. The fully dense EOS was calculated from DFT-MD, and used to fit a Hugoniot and ultimately a Mie-Gruneisen form for use in CTH. The unreacted EOS was used in simulations to verify the simulations matched historical data. An ARB model for HNS originally parameterized by Kipp[54] was modified and employed in additional reactive simulations. Initial reactive simulations resulted in threshold flyer velocities that match experimental data. The trends seen when changing the PSD were also reproduced, with larger PSDs resulting in longer run distances. For the thin flyers used (11 μm), the SDT process was seen to be heterogeneous,

however, sustained impulse simulations are likely to show homogeneous behavior, as has been observed experimentally. These simulations provide valuable insight into the non-linear response of HE to initial conditions of microstructure and variability in microstructure, which in turn helps to understand trends in sensitivity threshold.

ACKNOWLEDGMENTS

The authors would like to thank Mel Baer, retired senior scientist at Sandia National Laboratories, for many fruitful discussions about the nature of shock waves and explosive initiation. Also David Damm for discussions on reactive behavior and valuable suggestions for model development. This work was performed, in part, at the Center for Integrated Nanotechnologies, an Office of Science User Facility operated for the U.S. Department of Energy (DOE) Office of Science. Sandia National Laboratories is a multimission laboratory managed and operated by National Technology and Engineering Solutions of Sandia LLC, a wholly owned subsidiary of Honeywell International Inc. for the U.S. Department of Energy?s National Nuclear Security Administration under contract DE-NA0003525.

---

* cdyarri@sandia.gov

[1] M. D. Salas, Shock Waves **16**, 477 (2007).

[2] J. Morris, I. Lomov, and L. Glenn, J. Geophys. Res.-Sol Ea **108** (2003).

[3] F. P. Bowden and A. D. Yoffe, *Initiation and growth of explosion in liquids and solids* (Cambridge University Press, 1952).

[4] B. Khasainov, B. Ermolaev, H.-N. Presles, and P. Vidal, Shock Waves **7**, 89 (1997).

[5] C. Honodel, J. Humphrey, W. RC, L. RS, and K. P, in *7th Symposium (International) on Detonation* (Naval Surface Weapons Center, 1981) pp. 425–434.

[6] A. Campbell, W. Davis, J. Ramsay, and J. Travis, Phys. Fluids **4**, 511 (1961).

[7] R. Lee, G. Bloom, W. V. Holle, R. Weingart, L. Erickson, and S. Sanders, in *8th Symposium (International) on Detonation* (Naval Surface Weapons Center, 1985) pp. 3–14.

[8] C. L. Mader, Phys. Fluids **8**, 1811 (1965).

[9] C. L. Mader, in *5th Symposium (International) on Detonation* (Office of Naval Research, 1970) pp. 177–184.

[10] R. Williamson, J. Appl. Phys. **68**, 1287 (1990).

[11] D. J. Benson and W. J. Nellis, in *AIP Conf. Proc.*, Vol. 309 (AIP, 1994) pp. 1243–1246.

[12] M. Baer, R. Graham, M. Anderson, S. Sheffield, and R. Gustavsen, in *1996 JANNAF Combustion Subcommittee and Propulsion Systems Hazards Subcommittee Joint Meeting* (1996).

[13] M. R. Baer, AIP Conf. Proc. **505**, 27 (2000).

[14] M. Baer and W. Trott, in *12th International Detonation Symposium* (Office of Naval Research, 2002) pp. 939–950.

[15] M. Baer, Thermochim. acta **384**, 351 (2002).

[16] M. Baer, "Mesoscale modeling of shocks in heterogeneous reactive materials," in *ShockWave Science and Technology Reference Library*, edited by Y. Horie (Springer Berlin Heidelberg, 2007) Book section 8, pp. 321–356.

[17] J. Reaugh, in *13th International Detonation Symposium* (Office of Naval Research, 2006) pp. 1276–1285.

[18] A. Barua, S. Kim, Y. Horie, and M. Zhou, J. Appl. Phys. **113**, 064906 (2013).

[19] A. Barua, S. Kim, Y. Horie, and M. Zhou, J. Appl. Phys. **113**, 184907 (2013).

[20] S. Kim, C. Miller, Y. Horie, C. Molek, E. Welle, and M. Zhou, J. Appl. Phys. **120**, 115902 (2016).

[21] C. M. Tarver, S. K. Chidester, and A. L. Nichols, J. Phys. Chem. **100**, 5794 (1996).

[22] A. C. Schwarz, *Study of factors which influence the shock-initiation sensitivity of hexanitrostilbene (HNS)*, Report SAND80-2372 (Sandia National Labs., Albuquerque, NM (USA), 1981).

[23] A. Schwarz, in *7th Symposium (International) on Detonation* (Naval Surface Weapons Center, 1981) pp. 1024–1028.

[24] R. E. Setchell, Combust. Flame **56**, 343 (1984).

[25] S. M. Harris, S. E. Klassen, W. T. Quinlin, D. M. Cates, and R. Thorpe, "Aerospace sciences meetings," in *41st Aerospace Sciences Meeting and Exhibit* (American Institute of Aeronautics and Astronautics, 2003) Chap. Development of an ultrafine HNS for use in modern slapper detonators.

[26] A. L. Brundage, R. R. Wixom, A. S. Tappan, and G. T. Long, AIP Conf. Proc. **1195**, 315 (2009).

[27] J. McGlaun and S. Thompson, Int. J. Impact Eng. **10**, 10 (1990).

[28] A. Brundage, in *14th International Detonation Symposium* (Office of Naval Research, 2010) pp. 1051–1057.

[29] A. L. Brundage and J. C. Gump, AIP Conf. Proc. **1426**, 529 (2012).

[30] A. L. Brundage, in *ASME/JSME 2011 8th Thermal Engineering Joint Conference* (American Society of Mechanical Engineers, 2011) pp. T20095–T20095–10.

[31] A. Mattsson, R. Wixom, and T. Mattsson, in *14th International Detonation Symposium* (Office of Naval Research, 2010) pp. 1043–1050.

[32] D. L. Damm, R. R. Wixom, E. C. Dudley, C. D. Yarrington, and E. J. Welle, in *59th JANNAF Propulsion Meeting* (2012).

[33] E. Dudley, D. Damm, and E. Welle, in *14th International Detonation Symposium* (Office of Naval Research, 2010) pp. 622–630.

[34] M. W. Greenaway, M. J. Gifford, W. G. Proud, J. E. Field, and S. G. Goveas, AIP Conf. Proc. **620**, 1035 (2002).

[35] J. Waschl and D. Richardson, J. Energ. Mater **9**, 269 (1991).

[36] J. F. Jerier, B. Hathong, V. Richefeu, B. Chareyre, D. Imbault, F. V. Donze, and P. Doremus, Powder Technol. **208**, 537 (2011).

[37] K. J. Hanley, C. O'Sullivan, J. C. Oliveira, K. Cronin, and E. P. Byrne, Powder Technol. **210**, 230 (2011).

[38] N. Bourne and A. Milne, in *12th International Detonation Symposium* (Office of Naval Research, 2002) pp. 213–219.

[39] S. Torquato, *Random heterogeneous materials: microstructure and macroscopic properties*, Vol. 16 (Springer Science & Business Media, 2013).

[40] M. Knudson and M. Desjarlais, Phys. Rev. Lett. **103**, 225501 (2009).

[41] T. R. Mattsson, J. M. D. Lane, K. R. Cochrane, M. P. Desjarlais, A. P. Thompson, F. Pierce, and G. S. Grest, Phys. Rev. B **81**, 054103 (2010).

[42] R. R. Wixom, A. E. Mattsson, and T. R. Mattson, in *37th International Pyrotechnics Seminar (EUROPYRO 2011) and 10th international GTPS Seminar* (2011).

[43] R. Armiento and A. E. Mattsson, Phys. Rev. B **72**, 085108 (2005).

[44] G. Kresse and J. Hafner, Phys. Rev. B **47**, 558 (1993).

[45] G. Kresse and J. Hafner, Phys. Rev. B **49**, 14251 (1994).

[46] G. Kresse and J. Furthmüller, Phys. Rev. B **54**, 11169 (1996).

[47] A. E. Mattsson, P. A. Schultz, M. P. Desjarlais, T. R. Mattsson, and K. Leung, Model. Simul. Mater. Sc. **13**, R1 (2004).

[48] F. Gerard and A. Hardy, Acta Crystallogr. C **44**, 1283 (1988).

[49] E. Hertel and G. Kerley, *CTH EOS package*, Report SAND98-0945 (Sandia National Labs., Albuquerque, NM (USA), 1998).

[50] G. I. Kerley, in *8th Symposium (International) on Detonation* (Naval Surface Weapons Center, 1985) pp. 540–547.

[51] C. Yarrington, D. Kittell, R. Wixom, and D. Damm, J. Phys. Conf. Ser. **500**, 052053 (2014).

[52] D. E. Kittell and C. D. Yarrington, Combust. Theor. Model. **20**, 941 (2016).

[53] E. L. Lee and C. M. Tarver, Phys. Fluids **23**, 2362 (1980).

[54] M. Kipp and R. Setchell, in *9th Symposium (International) on Detonation*, Vol. 1 (Office of the Chief of Naval Research, 1989) pp. 209–218.

[55] R. E. Setchell, in *8th Symposium (International) on Detonation* (Naval Surface Weapons Center, 1985) pp. 15–25.